Gas, dust and stars in the SCUBA galaxy, SMM J02399−0136: the EVLA reveals a colossal galactic nursery

R. J. Ivison,[1,2]⋆ Ian Smail,[3] P. P. Papadopoulos,[4] I. Wold,[5] J. Richard,[3] A. M. Swinbank,[3] J.-P. Kneib[6] and F. N. Owen[7]

[1]*UK Astronomy Technology Centre, Science and Technology Facilities Council, Royal Observatory, Blackford Hill, Edinburgh EH9 3HJ*
[2]*Institute for Astronomy, University of Edinburgh, Blackford Hill, Edinburgh EH9 3HJ*
[3]*Institute for Computational Cosmology, Durham University, South Road, Durham DH1 3LE*
[4]*Argelander-Institüt für Astronomie, Auf dem Hügel 71, D-53121 Bonn, Germany*
[5]*Department of Astronomy, University of Wisconsin-Madison, 475 N. Charter St., Madison, WI 53706, USA*
[6]*Laboratoire d'Astrophysique de Marseille, OAMP, CNRS-Université Aix-Marseille, 38 rue Frédéric Joliot-Curie, 13388 Marseille Cedex 13, France*
[7]*National Radio Astronomy Observatory, PO Box 0, Socorro, NM 87801, USA*

ABSTRACT

We present new multiwavelength observations of the first submillimetre-selected galaxy (SMG) SMM J02399−0136 at $z = 2.8$. These observations include mapping of the CO $J=1\rightarrow0$ emission using elements of the Expanded Very Large Array, as well as high-resolution 1.4-GHz imaging and optical/infrared (IR) data from the Very Large Array, *Hubble Space Telescope*, *Spitzer* and Keck-I. Together, these new data provide fundamental insights into the mass and distribution of stars, gas and dust within this archetypal SMG. The CO $J=1\rightarrow0$ emission, with its minimal excitation and density requirements, traces the bulk of the metal-rich molecular gas, and reveals a molecular gas mass of $\sim10^{11}$ M$_\odot$, extending over approximately 5 arcsec ($\sim$25 kpc in the source plane), although there is tentative evidence that it may be significantly larger. Our data suggest that three or more distinct structures are encompassed by this molecular gas reservoir, including the broad absorption line (BAL) quasar from which the redshift of the SMG was initially determined. In particular, the new rest-frame near-IR observations identify a massive, obscured, starburst which is coincident with a previously known Lyα cloud. This starburst dominates the far-IR emission from the system and requires a re-assessment of previous claims that the gas reservoir resides in a massive, extended disc around the BAL quasi-stellar object (QSO). Instead, it appears that SMM J02399−0136 comprises a merger between a far-IR-luminous, but highly obscured starburst, the BAL QSO host and a faint third component. Our findings suggest that this archetypal SMG and its immediate environment mark a vast and complex galactic nursery and that detailed studies of other SMGs are likely to uncover a similarly rich diversity of properties.

Key words: galaxies: evolution – galaxies: high-redshift – galaxies: individual: SMM J02399−0136 – galaxies: starburst – infrared: galaxies – radio continuum: galaxies.

1 INTRODUCTION

Submillimetre- (submm-)selected galaxies (SMGs) were discovered using the Submm Common-User Bolometer Array (SCUBA – Holland et al. 1999), exploiting gravitational amplification by massive, foreground clusters (Smail, Ivison & Blain 1997; Smail et al. 2002). They are responsible for a significant fraction of the cosmic submm and far-infrared (far-IR) background (Fixsen et al. 1998)

and hence constitute an important class of distant galaxies. The Very Large Array (VLA) facilitated identification of the first SMGs, via high-resolution 1.4-GHz imaging (Ivison et al. 2000; Smail et al. 2000) enabling the acquisition of spectroscopic redshifts, e.g. $z = 2.8$ for the first SMG to be discovered, SMM J02339−0136 (hereafter SMM J02399) (Ivison et al. 1998, hereafter I98). The rest-frame ultraviolet (UV) spectral properties of SMM J02399 indicated that this system contained a low-ionization broad absorption line (BAL) quasar, denoted as L1 by I98, with a low surface brightness companion [possibly due to scattered active galactic nucleus (AGN) light], L2, associated with a large Lyα-emitting cloud,

⋆E-mail: rji@roe.ac.uk

extending over at least 20 kpc (I98; Ivison et al. 1999; Villar-Martín, Binette & Fosbury 1999; Vernet & Cimatti 2001). Vernet & Cimatti (2001) report an absorption complex at −1000 km s^{-1} and, for high-ionization lines, at −6700 km s^{-1}, both measured relative to L1 (at $z = 2.795$, which is ∼270 km s^{-1} blueward of L2). Mid-IR and X-ray data have suggested that the immense luminosity of this system, $L_{\rm bol} = 1.2 \times 10^{13} \, {\rm L_{\odot}}$, arises roughly equally from the AGN and starburst components (Bautz et al. 2000; Lutz et al. 2005; Valiante et al. 2007).

SMM J02399 was also the first SMG whose molecular gas was detected via CO (Frayer et al. 1998). This exploited the large positive K-correction afforded by even mildly excited high-J CO lines and the redshifting of their frequencies to transmissive parts of the atmosphere (see also Brown & Vanden Bout 1991, 1992; Solomon, Radford & Downes 1992; Solomon & Vanden Bout 2005). Since then, great progress has been made in discerning the H$_2$ gas mass distribution in distant SMGs, helping to characterize their evolutionary state (Frayer et al. 1999; Ivison et al. 2001); recently, more sensitive and higher resolution work has employed the Institut de Radioastronomie Millimétrique's (IRAM's) Plateau de Bure Interferometer (PdBI; Downes & Solomon 2003; Neri et al. 2003; Greve et al. 2005; Kneib et al. 2005; Tacconi et al. 2006, 2008). On the basis of CO $J=3{\rightarrow}2$ observations, Genzel et al. (2003), hereafter G03, argued for the presence of a massive and rapidly rotating disc in SMM J02399, associated with L1, although they could not rule out an alternative configuration with two galaxies orbiting one another. They reported a ∼3-arcsec structure in their sensitive rest-frame 335-μm continuum imaging, associating this with L1.

Only a handful of SMG studies (Greve, Ivison & Papadopoulos 2003; Hainline et al. 2006; Carilli et al. 2010) have made use of the CO $J=1{\rightarrow}0$ line – the transition most capable of tracing the bulk of the H$_2$ gas, with its minimal excitation requirements [$n_{\rm crit}({\rm H_2}) \sim 410 \, {\rm cm^{-3}}$ and E$_{10}$/k$_{\rm B} \sim 5.5$ K]. Instead, high-J (and thus high-excitation) CO transitions have usually been used. CO $J=3{\rightarrow}2$ and higher-J rotational levels probe the star-forming molecular gas (e.g. Zhu, Seaquist & Kuno 2003; Yao et al. 2003) and thus give a potentially biased view of the *total* gas mass and gas distribution.

It must be noted that even when it comes to the properties of the star-forming gas, comparisons between SMGs and local ultra-luminous infrared galaxies (ULIRGs) are difficult since the high-J CO lines routinely obtained for SMGs have only recently become available for the *global* molecular gas reservoirs of ULIRGs (e.g. Papadopoulos, Isaak & van der Werf 2007). Observations of the CO $J=1{\rightarrow}0$ line, on the other hand, allow the most straightforward estimate of metal-rich H$_2$ gas mass, its distribution and the enclosed galactic dynamical mass (assuming dynamically relaxed systems). Comparisons with the available CO $J=3{\rightarrow}2$ also allow an assessment of the global molecular gas excitation conditions, which are in turn a powerful indicator of the star-forming and non-star-forming molecular gas fractions in galaxies. The latter has been found to vary considerably, even among vigorous starbursts in the local Universe (Weiß, Walter & Scoville 2005) and at higher redshifts (e.g. Papadopoulos & Ivison 2002).

Here, we report sensitive new interferometric observations of SMM J02399, exploiting the arrival of Ka (26.5–40 GHz) Expanded VLA (EVLA) receivers at the VLA to trace the bulk of its molecular gas through its CO $J=1{\rightarrow}0$ line emission redshifted into a hitherto inaccessible frequency range (over half of radio-identified SMGs lie at $z = 1.88$– 3.35 corresponding to CO $J=1{\rightarrow}0$ in the Ka frequency band; Chapman et al. 2005). This well-studied and bright target provides an obvious starting point for future CO $J=1{\rightarrow}0$ surveys of the SMG population with EVLA. We also present sensitive, new

1.4-GHz continuum imaging, spectroscopic imaging in the rest-frame UV from the Keck-I telescope, and deep multifilter imaging with *Spitzer* and the Advanced Camera for Surveys (ACS) aboard the *Hubble Space Telescope* (*HST*).

Throughout this paper, we assume a flat cosmological model with $\Omega_\Lambda = 0.7$ and $H_0 = 70 \, {\rm km \, s^{-1} \, Mpc^{-1}}$.

2 OBSERVATIONS

2.1 CO $J=1{\rightarrow}0$ observations using the EVLA

Around 70 h of data were obtained with the VLA in its C configuration during 2009 July–September, around half via dynamically scheduled 2-h blocks, the rest via fixed 6-h blocks. The weather conditions were generally excellent. We discarded 20 h of data, taken when a pointing bug was affecting the array, and around 6 h of data, taken when the weather was unsuitable.

A compact calibrator, 0239−025 (1.0 Jy at 30.3 GHz), lies ∼1° from SMM J02399, and we used this to track the phase and amplitude every 3–5 min, as well as to update the VLA's pointing model every hour (at 8.4 GHz). 0137+331 (3C 48) was used to calibrate the flux density scale.

Typically, around 10 receivers were functional at any one time, each mounted on an upgraded EVLA antenna. We used continuum mode, giving dual-polarization channels, each with a bandwidth of 50 MHz (or ∼500 km s^{-1} for CO $J=1{\rightarrow}0$ at $z \sim 2.805$). The observed frequency of the CO $J=1{\rightarrow}0$ transition lies below 32 GHz for $z \sim 2.8$, where only two intermediate frequencies (IFs), B and D, can be tuned; so we placed IFs A and C at 32.3 GHz to constrain the off-line flux density, even though we expected no significant continuum emission from either the synchrotron, the free–free or the dust (I98). We alternated the tuning of IFs B and D between the blue and red peaks seen by Frayer et al. (1998) and G03, although some data were taken at non-optimal frequencies.

The data were processed using standard AIPS procedures developed for high-frequency observation. Our calibration strategy was able to track changes in phase and amplitude accurately across the full 0–300 kλ of uv coverage. Imaging was accomplished using IMAGR within AIPS.

2.2 CO $J=3{\rightarrow}2$ and 1.3-mm continuum observations

G03's 1.3-mm continuum imaging of SMM J02399 from IRAM's PdBI, and their CO $J=3{\rightarrow}2$ data cube, were kindly made available to us by L. Tacconi and A. Baker (private communication). We use these data here to facilitate the most complete possible picture of the molecular gas in SMM J02399 and its physical conditions. The 1.3-mm imaging yields a beam of 1.8×1.4 arcsec^2 (very close to that of our 1.4-GHz radio map, see Section 2.3), while the CO $J=3{\rightarrow}2$ map has significantly lower resolution, 5.2×2.4 arcsec^2. A full description of the observations and their reduction is given in G03.

2.3 1.4-GHz imaging with the Very Large Array

Data at 1.4 GHz were obtained for the Abell 370 cluster field during August and September in both 1994 (B configuration) and 1999 (A), recording 7×3.125-MHz channels in each of the two dual-polarization IF pairs. 0259+077 (B) and 0323+055 (A) were used to track amplitude and phase and 0137+331 was used for flux and bandpass calibration. Data processing and imaging followed

the description given by Owen & Morrison (2008). The resulting continuum map has a noise level of ∼5.7 μJy beam^{-1} near SMM J02399, with a 1.8×1.6-arcsec^2 synthesized beam (position angle, PA, 166°).

2.4 *Hubble Space Telescope* and *Spitzer* observations

Following the successful Servicing Mission #4 in 2009 May, observations were obtained using the ACS during 2009 July (PID 11507), for a total of 6780, 2040 and 3840 s in the F475W (*g*), F625W (*r*) and F814W (*i*) bands, respectively. The data were reduced using the MULTIDRIZZLE package and the images are available. [1]

In addition, we have retrieved Near Infrared Camera and Multi-Object Spectrometer (NICMOS) imaging of SMM J02399 (PID 11143). These were reduced and combined in the standard manner from the pipeline-reduced data in the Space Telescope European Coordinating Facility archive. They comprise 2560 s of integration with the NIC2 camera in the F110W (*J*) and F160W (*H*) filters.

Finally, Abell 370 was observed with *Spitzer* (Werner et al. 2004) in all the IR Array Camera (IRAC – Fazio et al. 2004) bands (3.6–8.0 μm) in 2006 February (PID: 137). The total integration time was 9 ks in each of the four bands: 3.6, 4.5, 5.8 and 8 μm.

2.5 Keck spectroscopic observations

Keck-I long-slit spectroscopy was obtained during 2001 October using LRIS (Oke et al. 1995) to step through seven positions across the object, integrating for 2 ks in each, with a 1-arcsec slit and the low-resolution 300 lines mm^{-1} grism. A full description of the observations and data reduction are presented in Santos et al. (2004).

2.6 Astrometric alignment

The bright point source, L1, visible in many wavebands, has allowed us to remove the positional ambiguity that would otherwise hamper a detailed comparison of the kind undertaken here.

We adopt the VLA 1.4-GHz map as our fundamental coordinate frame and shift the other frames to this one to align the emission from L1. We employed local phase calibrators (1.̊0, 10.̊6 and 13.̊0 from SMM J02399), with positions known to ∼1 mas, and residual phase errors after calibration were small, so we estimate the absolute alignment of the 1.4-GHz and CO $J=1\rightarrow0$ coordinate frames should be better than 0.1 arcsec, leaving aside uncertainties relating to signal-to-noise ratio and beam size (discussed in Section 3.4). The astrometry of the *HST* images was first calibrated against a wider field optical image of the cluster which had in turn been aligned on to the FK5 coordinate system defined by United States Naval Observatory optical catalogue to an rms precision of ∼0.2 arcsec. To align the IRAM data (1.3-mm continuum and CO $J=3\rightarrow2$) with the 1.4-GHz continuum emission, we shifted the former to the east by 0.5 arcsec in RA, which is consistent with the claimed astrometric precision of the PdBI images. To align the optical/near-IR data with the 1.4-GHz continuum emission, we shifted the former in Dec. by +0.15 arcsec.
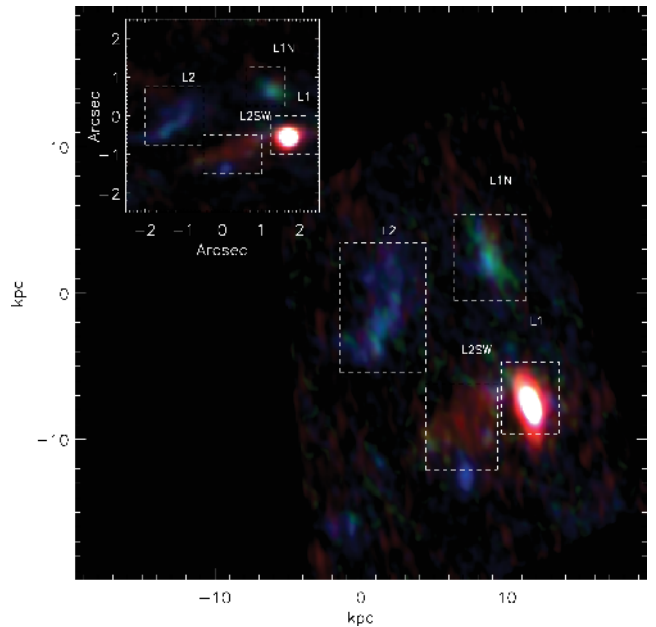
Figure 1. True-colour representations of the *HST*/ACS SM4 ERO and NICMOS observations of SMM J02399 (comprising F475W, F625W and F160W exposures) as seen before (inset) and after (main panel) correcting for the gravitational lensing model described in Section 2.7. In the rest-frame UV imaging, we identify the BAL QSO, L1, as well as a marginally extended and somewhat bluer companion, L1N, and the much bluer L2. In contrast, the NICMOS image identifies an extended source, L2SW, which is very red in the rest-frame UV–optical. This source appears to coincide with the far-IR-bright and gas-rich emission region within this system. These four primary emission regions are marked.

2.7 The lensing model

Having described the large collection of new and archival data at our disposal, we describe now how we deal with the gravitational lensing experienced by SMM J02399. We correct for the lensing distortion and magnification using a mass model of the Abell 370 cluster. This is discussed in detail by Richard et al. (2010) and is based on 10 multiply-imaged systems detected in the *HST*/ACS data (Section 2.4). We derive a total magnification factor of 2.38 ± 0.08 at the location of SMM J02399 in a direction roughly aligned with L1–L2 and we use the model to reconstruct the morphology in the source plane using LENSTOOL (Kneib et al. 1996). The effect of the correction can be seen in Fig. 1.

3 ANALYSIS AND RESULTS

3.1 Taxonomy

We begin with a brief description of the SMM J02399 system, as seen in the rest-frame UV–optical true-colour imaging from *HST*. In what follows, we will refer to four main components seen in Fig. 1: L1 – the BAL quasar to the west, the brightest UV emitter in the region; L1N – the bright, compact source, ∼8 kpc north of L1; L2 – the low surface brightness feature, ∼10 kpc east of L1; L2SW, the red feature seen in our NICMOS imaging extending ∼6 kpc to the south-east of L1.
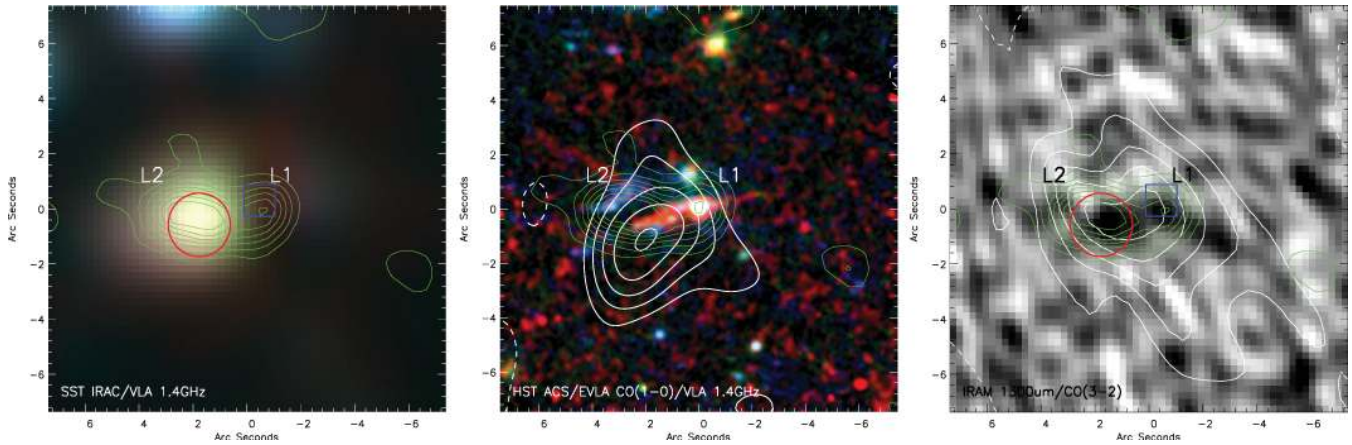
Figure 2. Left: a true-colour 3.6, 4.5 and 5.8-μm image of SMM J02399, where we have removed the contribution from L1 by scaling and subtracting a point source from each of the bands, revealing emission coincident with L2SW. We overlay on this the 1.4-GHz continuum contours (green) and the positions of the 850-μm and X-ray centroids (red circle – I98; blue square – Bautz et al. 2000, as revised by G03). Middle: CO $J=1\rightarrow0$ (white contours) from an image made with a Gaussian taper of 50 kλ, plus 1.4-GHz continuum (green), overlaid on the *HST* imaging. CO contours: $-3, -2, 2, 3, 4, 5, 6\sigma$, where $\sigma = 50$ μJy beam^{-1}; 1.4-GHz: $-4, -2, 2, 4, 6, 8, 10\sigma$, where $\sigma = 5.7$ μJy beam^{-1}. Right: contours (white) of the CO $J=3\rightarrow2$ velocity-integrated emission superimposed on a grey-scale image of the 1.3-mm continuum emission (G03). G03 suggested that L1 is the primary repository of SMM J02399's dust and gas. It is clear that the dusty gas reservoir is not centred on L1, but is coincident with L2SW – the very red source highlighted by the NICMOS imaging.

3.2 Radio continuum morphology

In Fig. 2 (central panel), we see the 1.4-GHz synchrotron emission overlaid as green contours on the *HST* true-colour image, together with 50-kλ-tapered CO contours. A knot of synchrotron emission is coincident with L1 but the majority of the radio emission extends to the east, close to the extended near-IR source, L2SW. It is coincident to within the uncertainties with the original SCUBA 850-μm continuum centroid, with the PdBI 1.3-mm continuum emission, and with the CO $J=3\rightarrow2$ line emission (I98; G03), as shown in the right-hand panel of Fig. 2.

There are two possible explanations for the radio morphology of this system. First, the radio morphology could be due to a bipolar jet from L1 – a known X-ray-bright BAL quasar – which encounters only one working surface: the cloud of molecular gas traced by the CO and dust emission, to the east of L1. In this scenario, L2 and L2SW may be shock-excited regions – L2 lying at the point where the jet terminates – with the entire system powered by the kinetic energy of the jet (e.g. Punsly & Tingay 2005). Taking this interpretation, SMM J02399 is reminiscent of the system described by Józsa et al. (2009), where extended emission originating at the centre of IC 2497 at $z = 0.05$, probably a radio jet, points in the direction of Hanny's Voorwerp – a region in a neighbouring H I cloud, first seen because of its shock-excited, optical emission lines.

Alternatively, and more plausibly, the extended emission may be associated with a heavily dust-obscured starburst between L1 and L2. As we shall see in the next section, the host of this starburst, L2SW, is identified through IRAC and NICMOS rest-frame optical/near-IR emission, as well as wispy rest-frame UV emission structures representing leakage from patches of low obscuration (similar to the scenario proposed for SMM J14011+0252 by Ivison et al. 2001). The spatial coincidence of this source with the CO reservoir, as well as the 850-μm and 1.3-mm continuum emission, strongly suggests it is the seat of the hyperluminous starburst within this system.

As an aside, the lack of emission at 32.3 GHz rules out the possibility that the AGN within L1 has a flat-spectrum core.

3.3 Rest-frame UV/optical/near-IR light

The most remarkable feature of the 2D spectroscopy described in Section 2.5 is that Lyα is seen across the entire 1600-kpc^2 region shown in Fig. 1. The scale of the Lyα nebular was hinted at by early data (I98) but we can see now that SMM J02399 is a classic 'Lyα blob' (e.g. Matsuda et al. 2004). There is a velocity gradient in Lyα as one moves from L1 to L2. Secondary peaks in Lyα intensity and velocity dispersion are coincident with L2 – the local velocity gradient is around ~500 km s^{-1}. UV continuum is cospatial with the line emission over much of the region, but none is seen near L2.

Fig. 3 shows 1D spectra of the four regions identified in Fig. 1. Strong Lyα and N v emission dominate the spectrum of L1, along with weak He II ($\lambda164.5$ nm) (e.g. I98) at 625.17 ± 0.20 nm. L2 and L2SW are practically indistinguishable spectroscopically. Regarding the Lyα emission, and the proximity of an AGN/starburst, SMM J02399 is very similar to the Lyα nebula presented by Scarlata et al. (2009). L1N, L2 and L2SW all show weak N v emission suggesting that they contain ionizing sources.

L1 dominates the SMM J02399 system in IRAC wavebands. We show in the left-hand panel of Fig. 2 the true-colour IRAC image after subtraction of a point source at the position of L1. It is immediately apparent that L2SW emits strongly at rest-frame 0.95–1.5 μm.

Using the optical photometry from I98 and the flux densities of L2 determined from the NICMOS and IRAC imaging (Section 2.4; see also Figs 1 and 2), we find that the spectral energy distribution (SED) is well fitted with a reddened and very young stellar population ($A_V \sim 1.5$; ~10 Myr old). From this, we derive a best-fitting, rest-frame, lensing-corrected *H*-band luminosity for the galaxy, $M_H \sim -25.4$, equivalent to a stellar mass of ~10^{11} M$_\odot$ using a light-to-mass ratio appropriate for a young burst ($L_H/M \sim 3$), with an uncertainty of at least a factor of 3 times (Borys et al. 2005). This confirms the visual impression (Fig. 2) that L2 corresponds to a massive stellar system. We note that the rest-frame 1.5–2 μm SED of L2 is flat, suggesting that an obscured AGN is not dominating its near-IR luminosity (cf. Hainline et al., in preparation). We stress that the combined SED of L1 and L2 is dominated by the AGN
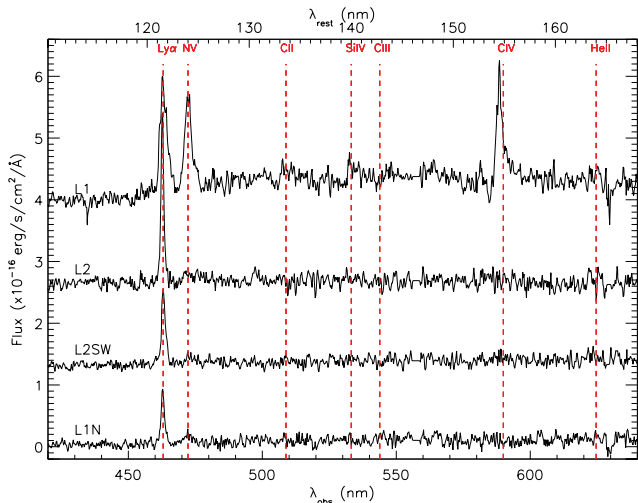
Figure 3. Keck/LRIS spectroscopy of the four regions identified in Fig. 1. All four regions display strong Lyα emission and – with the exception of L1 – weak or undetected rest-frame UV continuum emission. The spectrum of L1 displays the strong, self-absorbed emission lines characteristic of BAL QSOs. The three other regions display Lyα and weak N v emission, suggesting local ionization sources may reside in these components. The wavelengths of potential emission features are marked.

Figure 4. Amplitude of the real visibility components as a function of baseline length. The amplitude of the imaginary components, whose 1σ range is indicated in grey, is consistent with zero. A Gaussian consistent with a source size of 10 kλ (20 arcsec full width at half-maximum) is shown to guide the eye.

emission from L1. Only the combination of gravitational lensing and the high-resolution imaging used here allows us to decouple the AGN activity from that of the luminous, obscured starburst within this system. Similarly, detailed studies of other SMGs may also uncover a rich variety in their properties (e.g. Ivison et al. 2000, 2008).

3.4 Molecular gas

The other major baryonic component in the system is the cold gas. The CO $J=1\rightarrow0$ images mentioned in Section 2.1 were made using a variety of Gaussian uv tapers (125, 75 and 50 kλ) resulting in synthesized beam sizes of ∼1.7, 2.4 and 3.2 arcsec and noise levels of 26–50 μJy beam^{-1}. The noise level rises as the longer baselines are weighted down, but the signal due to CO line emission increases markedly. This is best illustrated by the amplitudes of the real and imaginary visibility components (Fig. 4) which suggest that the CO emission is resolved on baselines longer than ∼10 kλ, with a total flux density of approximately 500 μJy.

The position of the CO $J=1\rightarrow0$ emission ($02^h39^m51^s96 \pm 0^s03$, $-01°36'59''8 \pm 0''5$ J2000; see Fig. 2) is consistent with the emission seen by SCUBA and PdBI. We cannot rule out a contribution to the CO $J=1\rightarrow0$ flux from the quasar, but the majority of the emission appears to be coincident with L2SW.

The peak and total flux densities in the most severely tapered CO $J=1\rightarrow0$ map are 325 ± 50 and 540 ± 150 μJy. The latter value is sensitive to the manner in which the measurement is made; however, Gaussian fits and a simple integral over the emission region in the dirty image with TVSTAT give results consistent with Fig. 4. We adopt 540 μJy as the total CO $J=1\rightarrow0$ flux density hereafter. Gaussian fits to the dirty image provide a very rough indication of the size of the emission region: 2.0×5.0 arcsec^2, with the major axis at PA, $150° \pm 20°$, implying a lensing-corrected size of ∼25 kpc. This is only barely consistent with the uv visibilities (which suggest a size closer to 10 arcsec). Without data from the VLA in its D
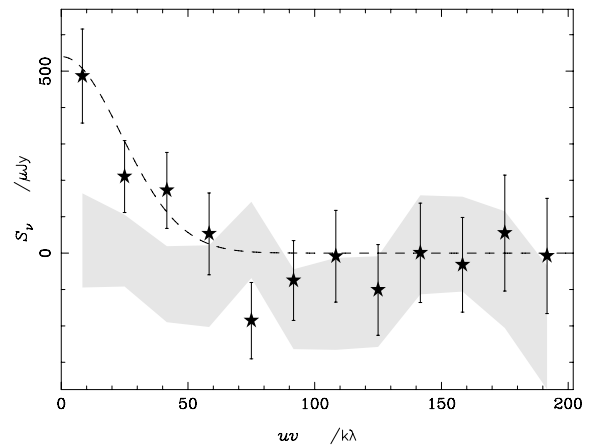
configuration, we have only loose constraints on the size of the CO $J=1\rightarrow0$ emitting region and may be underestimating the total flux density.

To correct for the finite throughput of our IFs, we adopt and adapt the strategy of Greve et al. (2003), correcting upwards by 45 per cent to account for the breadth of the line seen by G03 relative to our total bandwidth (∼90 MHz, taking into account the bandpass rollover), which takes the total flux in CO $J=1\rightarrow0$ to $S_{1-0} \, dV = 0.70 \pm 0.18$ Jy km s^{-1}.

As expected, no signal is apparent in the 'off-line' IF pair, down to a 2σ limit of $S_{32.3\,GHz} < 60$ μJy. This situation does not change when tapering the uv data, although the noise doubles when a 50-kλ taper is applied.

The velocity/area-integrated CO brightness temperature in the source reference frame, $L_{1-0} = \int_{\Delta V} \int_{A_s} T_b \, dA \, dV$, can be expressed as

$$L_{1-0} = \frac{3.25 \times 10^7}{(1+z)} \left(\frac{D_L}{\nu_{CO}}\right)^2 \int S_{1-0} \, dV \text{ K km s}^{-1} \text{ pc}^2, \qquad (1)$$

where D_L is the luminosity distance (Mpc), ν_{CO} is the rest-frame frequency (GHz) of the CO $J=1\rightarrow0$ transition and the velocity-integrated flux density is in Jy km s^{-1} (e.g. Solomon et al. 1997). The corresponding H$_2$ mass, $M(H_2)$, is given by $X_{CO}L_{1-0}$, where X_{CO} is the CO–H$_2$ luminosity–mass conversion factor. For quiescent environments, $X_{CO} \sim 5$ M$_\odot$ (K km s^{-1} pc^2)$^{-1}$ (e.g. Solomon et al. 1987; Solomon & Barrett 1991). In extreme starburst environments, like those prevailing in SMM J02399, $X_{CO} \sim 1$ M$_\odot$ (K km s^{-1} pc^2)$^{-1}$ may be more suitable (Downes & Solomon 1998), which corrects semi-empirically for the fact that the molecular gas reservoir in the dissipative mergers that typically characterize such starbursts is a continuous medium with a significant stellar mass component rather than an ensemble of virialized clouds (so that CO linewidths no longer reflect only the mass of gas). In this case, $M(H_2) \sim (1.0 \pm 0.3) \times 10^{11}$ M$_\odot$ (after correcting for lensing amplification).

An absolute lower limit for the H$_2$ gas mass can be obtained by assuming that the ^{12}CO $J=1\rightarrow0$ emission is optically thin. For local

thermodynamic equilibrium,

$$\frac{M(\mathrm{H_2})}{L_{1-0}} \sim 0.08 \left\{ \frac{g_1}{Z} e^{-T_\circ/T_k} \left[\frac{J(T_k) - J(T_{bg})}{J(T_k)} \right] \right\}^{-1}$$
$$\times \left(\frac{[\mathrm{CO/H_2}]}{10^{-4}} \right)^{-1} \frac{\mathrm{M_\odot}}{\mathrm{K\,km\,s^{-1}\,pc^2}}, \qquad (2)$$

where $T_\circ = E_1/k_B \sim 5.5\,\mathrm{K}$, $J(T) = T_\circ(e^{T_\circ/T} - 1)^{-1}$, $T_{bg} = (1 + z)T_{CMB} \sim 10\,\mathrm{K}$ (the temperature of the cosmic microwave background at $z = 2.8$), $g_1 = 3$ – the degeneracy of level $n = 1$, $Z \sim 2(T_k/T_\circ)$ – the partition function and $[\mathrm{CO/H_2}] \sim 10^{-4}$ for a solar metallicity environment (Bryant & Scoville 1996). For typical star-forming gas, where $T_k \sim 40\text{--}60\,\mathrm{K}$, this yields $\langle X_{CO}^{thin} \rangle \sim 0.65\,\mathrm{M_\odot}\,(\mathrm{K\,km\,s^{-1}\,pc^2})^{-1}$, and thus $M(\mathrm{H_2})_{min} \sim 6 \times 10^{10}\,\mathrm{M_\odot}$ is the minimum plausible molecular gas mass in this system. Of course, CO traces metal-rich gas and in metal-poor environments (and/or intense far-UV radiation fields) more molecular gas may be present where CO has been dissociated. In this sense, and because we cannot rule out that we have missed a more extensive CO $J=1\rightarrow0$ component due to the lack of D-configuration EVLA data, the latter value is a firm lower limit.

The availability of both CO $J=1\rightarrow0$ and $J=3\rightarrow2$ allows a rudimentary probe of the average molecular gas excitation state. This can provide powerful clues about whether a galaxy-wide starburst occurs over most of the available molecular gas reservoir (pushing the global r_{3-2} ratio up), or whether a smaller gas mass fraction is involved in fuelling the starburst. High global high-J/low-J CO line ratios, indicative of galaxy-wide starbursts involving most of the ambient gas reservoir, have been observed in various high-redshift systems (e.g. Papadopoulos et al. 2005; Weiß et al. 2007), but low ratios in vigorously starbursting systems have also been detected (Papadopoulos & Ivison 2002; Daddi et al. 2009; Dannerbauer et al. 2009).

For the reported CO $J=3\rightarrow2$ velocity-integrated line flux of $I_{3-2} = \int S_{3-2}\,\mathrm{d}V = 3.0 \pm 0.3\,\mathrm{Jy\,km\,s^{-1}}$ (Frayer et al. 1998; G03), the globally average CO $(3-2)/(1-0)$ brightness temperature ratio would be $r_{3-2/1-0} = (\nu_{1-0}/\nu_{3-2})^2\,(I_{3-2}/I_{1-0}) = 0.48 \pm 0.13$. This line ratio is well within the domain expected for globally star-forming molecular gas, although it lies towards the low end of the expected range. Quiescent Milky Way clouds have $r_{3-2/1-0} \sim 0.2 - 0.3$ whilst the typical average value for starburst nuclei is $r_{3-2/1-0} = 0.65$ (Devereux et al. 1994; Yao et al. 2003). A grid of radiative transfer large-velocity gradient (LVG) models, constrained by the observed ratio and $T_k \geq T_{dust}$ (since gas is always warmer than the concomitant dust where the gas is heated by far-UV radiation and/or turbulence), with the latter being $T_{dust} \gtrsim 40\,\mathrm{K}$ (I98) yields $n(\mathrm{H_2}) \sim 300\text{--}10^3\,\mathrm{cm^{-3}}$, for $T_k = 40 - 110\,\mathrm{K}$, for various values of the average gas velocity gradient $\mathrm{d}V/\mathrm{d}r$. Given that other CO line ratios are not available to us, there is an irreducible $n(\mathrm{H_2}) - T_k$ degeneracy (the higher the temperature, the lower the density reproducing a given CO ratio, typically). If we further constrain the LVG solutions by allowing only those corresponding closely to virialized molecular gas velocity fields where

$$K_{vir} = \frac{(\mathrm{d}V/\mathrm{d}r)_{obs}}{(\mathrm{d}V/\mathrm{d}r)_{vir}} \sim 1.54 \frac{[\mathrm{CO/H_2}]}{\sqrt{\alpha}\,\Lambda_{CO}} \left[\frac{\langle n(\mathrm{H_2}) \rangle}{10^3\,\mathrm{cm^{-3}}} \right]^{-1/2} \sim 1, \qquad (3)$$

where $K_{vir} \gg 1$ and $K_{vir} < 1$ correspond to unbound gas motions and unphysical subvirial motions, respectively, we find that the solutions with $T_k \sim 45\text{--}50\,\mathrm{K}$ are mostly favoured. We note, however, that supervirial solutions are plausible if the CO $J=1\rightarrow0$ emission originates predominantly from a cold, extended gas reservoir; indeed, $K_{vir} \gg 1$ solutions occupy the majority of the $n(\mathrm{H_2}) - T_k$

parameter space compatible with the observed line ratio, typically with $n(\mathrm{H_2}) \sim 10^3\,\mathrm{cm^{-3}}$ and $T_k \sim 55\text{--}90\,\mathrm{K}$, conditions that often characterize the gas in starbursts (e.g. Aalto et al. 1995).

4 DISCUSSION AND CONCLUDING REMARKS

Based on the rest-frame UV and optical imaging, it appears that the SMM J02399 system comprises at least three significant components: L1, L1N and L2SW. Are these all massive baryonic galaxies within a very large reservoir of molecular gas, each caught during a different phase of their development? Or does L1 dominate the system, with L2SW, L1N (and L2) representing mere outflows and reflections?

G03 argued that the dust and gas seen towards SMM J02399 are associated with L1 and that the dynamics of the system as a whole are best described as a massive disc. Based on the data described here and elsewhere, there is little doubt that L1 does represent a significant concentration of mass: it is the brightest rest-frame UV emitter in the region; it is bright in the rest-frame 0.95–2.1 μm waveband and hosts an X-ray-bright BAL quasar. However, Fig. 2 suggests that G03's main assertion may not be correct because the mm/submm, radio and CO emission lie predominantly on and around L2SW, although some weak emission does appear to be associated with L1.

Moving on to L2 and L2SW, Vernet & Cimatti (2001) and G03 argued that L2 is due to scattered light from L1, although G03 did concede that the L1/L2 system may comprise two galaxies orbiting one another. As we have argued, the true-colour *Spitzer* imaging presented in Fig. 2 shows that *L2SW is a luminous source at rest-frame 0.95–1.5 μm.* We stress that several of these bands are not expected to suffer strong contamination by emission lines; hence, we are seeing continuum emission, not scattered light.

We conclude that SMM J02399 comprises at least two galaxies – possibly as many as four – caught at different points during their evolution. In the evolutionary scheme outlined by Page et al. (2004), L1N may be the most evolved of these systems, followed by L1, L2 and the gas- and dust-rich system, L2SW, whose rest-frame far-IR emission led to the system's discovery. However, this sequence could just as easily be related to mass: we have either one or two UV systems with modest stellar mass, the quasi-stellar object (QSO) host galaxy, which must be massive according to Magorrian et al. (1998), plus a massive, obscured starburst.

The major result from our study is the discovery of a massive, cold and apparently extended gas reservoir in SMM J02399. Tentative evidence for luminous CO $J=1\rightarrow0$ emission in SMGs had been published previously (Greve et al. 2003; Hainline et al. 2006). Greve et al. used the VLA to observe ERO J16452+4626.4, a submm-bright starburst at $z = 1.4$, finding $r_{2-1/1-0} = 0.6 \pm 0.2$ and $r_{5-4/1-0} = 0.10 \pm 0.05$. Similarly, Hainline et al. observed the AGN-dominated $z = 3.4$ SMG, SMM J13120+4242, using the Green Bank Telescope, and found a brightness temperature ratio, $r_{4-3/1-0} = 0.26 \pm 0.06$, indicative of a massive, subthermally excited molecular gas reservoir. Our new observations suggest that massive, cold gas components must be common amongst the SMG population.

In retrospect this discovery should not come as a great surprise. As is widely appreciated, optical/IR lines can lead to misleading views of velocity fields and galaxy types/sizes. They trace ionized gas, whose distribution traces the star formation and AGN activity within the galaxy, rather than its underlying structure. Equally, however, the excitation requirements of high-J CO lines tie them to a particular star formation area, so they do not give a faithful

picture of the true H_2 mass and dynamical mass distributions in galaxies either. The compact ($\sim$0.5–1 kpc) emitting regions thereby revealed (Tacconi et al. 2008) are unlikely to trace the true dimensions of galaxies. It can be argued that high-*J* observations simply return the star formation efficiency (SFE) per *star-forming* H_2 gas mass, rather than the more fundamental SFE per *total* H_2 gas mass. Indeed, previous high-*J* CO studies have uncovered low $r_{6-5/3-2}$ and $r_{7-6/3-2}$ brightness temperature ratios ($\sim$0.15–0.35) in several SMGs (Tacconi et al. 2006) and such a low global high-*J*/low-*J* CO ratio is exactly how a massive, low-excitation H_2 gas phase would betray itself at high redshifts.

A similar situation exists at $z \sim 0$ where low-excitation H_2 gas is found to extend well beyond compact nuclear starbursts (e.g. Weiß et al. 2005) while containing the *bulk* of the H_2 gas mass. Line ratios comparable to those seen in the SMGs can be recovered by degrading similar observations of local starbursts and vigorously star-forming spirals (see Papadopoulos & Seaquist 1998) to the spatial resolution typically available in CO observations of the distant Universe (1–10 kpc).

The confirmation of the presence of significant amounts of cold gas in SMGs has several significant implications for the interpretation of this population. In particular, the large gas reservoir detected in CO $J=1\rightarrow0$ highlights the danger of drawing far-reaching conclusions from more biased high-*J* studies, particularly concerning the gas mass and gas fraction, the dynamics of SMGs, the evolutionary links between SMGs and their likely descendants at $z \sim 0$, their true star-forming potential (i.e. their potential present-day mass), the possible durations of star-forming episodes and the state of their velocity fields (ordered and/or disc-like versus the more chaotic fields typical of mergers) – *all* of these issues are important, yet the answers remain largely unknown.

In the fullness of time, we expect EVLA, the Atacama Large Millimetre/submm Array and the *Herschel Space Observatory* to fully compare the excitation properties of gas reservoirs in SMGs, ULIRGs and QSOs and the relative distributions of star-forming and quiescent molecular gas, relating this to the activity in these systems, and their evolution, thereby constraining theoretical models of galaxy formation (Swinbank et al. 2008).

ACKNOWLEDGMENTS

REFERENCES

Aalto S., Booth R. S., Black J. H., Johansson L. E. B., 1995, A&A, 300, 369
Bautz M. W., Malm M. R., Baganoff F. K., Ricker G. R., Canizares C. R., Brandt W. N., Hornschemeier A. E., Garmire G. P., 2000, ApJ, 543, L119
Borys C., Smail I., Chapman S. C., Blain A. W., Alexander D. M., Ivison R. J., 2005, ApJ, 635, 853
Brown R. L., Vanden Bout P. A., 1991, AJ, 102, 1956
Brown R. L., Vanden Bout P. A., 1992, ApJ, 397, L19
Bryant P. M., Scoville N. Z., 1996, ApJ, 457, 678
Carilli C. L. et al. 2010, ApJ, submitted
Chapman S. C., Blain A. W., Smail I., Ivison R. J., 2005, ApJ, 622, 772
Daddi E. et al., 2009, preprint (arXiv:0911.2776)
Dannerbauer H., Daddi E., Riechers D. A., Walter F., Carilli C. L., Dickinson M., Elbaz D., Morrison G. E., 2009, ApJ, 698, L178
Devereux N., Taniguchi Y., Sanders D. B., Nakai N., Young J. S., 1994, AJ, 107, 2006
Downes D., Solomon P. M., 1998, ApJ, 507, 615
Downes D., Solomon P. M., 2003, ApJ, 582, 37
Fazio G. G. et al., 2004, ApJS, 154, 10
Fixsen D. J., Dwek E., Mather J. C., Bennett C. . L., Shafer R. A., 1998, ApJ, 508, 123
Frayer D. T., Ivison R. J., Scoville N. Z., Yun M., Evans A. S., Smail I., Blain A. W., Kneib J., 1998, ApJ, 506, L7
Frayer D. T. et al., 1999, ApJ, 514, L13
Genzel R., Baker A. J., Tacconi L. J., Lutz D., Cox P., Guilloteau S., Omont A., 2003, ApJ, 584, 633 (G03)
Greve T. R., Ivison R. J., Papadopoulos P. P., 2003, ApJ, 599, 839
Greve T. R. et al., 2005, MNRAS, 359, 1165
Hainline L. J., Blain A. W., Greve T. R., Chapman S. C., Smail I., Ivison R. J., 2006, ApJ, 650, 614
Holland W. S. et al., 1999, MNRAS, 303, 659
Ivison R., Smail I., Blain A., Kneib J., Frayer D., 1999, Ap&SS, 266, 285
Ivison R. J., Smail I., Le Borgne J., Blain A. W., Kneib J., Bezecourt J., Kerr T. H., Davies J. K., 1998, MNRAS, 298, 583 (I98)
Ivison R. J., Smail I., Barger A. J., Kneib J., Blain A. W., Owen F. N., Kerr T. H., Cowie L. L., 2000, MNRAS, 315, 209
Ivison R. J., Smail I., Frayer D. T., Kneib J., Blain A. W., 2001, ApJ, 561, L45
Ivison R. J. et al., 2008, MNRAS, 390, 1117
Józsa G. I. G. et al., 2009, A&A, 500, L33
Kneib J., Ellis R. S., Smail I., Couch W. J., Sharples R. M., 1996, ApJ, 471, 643
Kneib J., Neri R., Smail I., Blain A., Sheth K., van der Werf P., Knudsen K. K., 2005, A&A, 434, 819
Lutz D., Yan L., Armus L., Helou G., Tacconi L. J., Genzel R., Baker A. J., 2005, ApJ, 632, L13
Magorrian J. et al., 1998, AJ, 115, 2285
Matsuda Y. et al., 2004, AJ, 128, 569
Neri R. et al., 2003, ApJ, 597, L113
Oke J. B. et al., 1995, PASP, 107, 375
Owen F. N., Morrison G. E., 2008, AJ, 136, 1889
Page M. J., Stevens J. A., Ivison R. J., Carrera F. J., 2004, ApJ, 611, L85
Papadopoulos P. P., Ivison R. J., 2002, ApJ, 564, L9
Papadopoulos P. P., Seaquist E. R., 1998, ApJ, 492, 521
Papadopoulos P. P., Greve T. R., Ivison R. J., De Breuck C., 2005, A&A, 444, 813
Papadopoulos P. P., Isaak K. G., van der Werf P. P., 2007, ApJ, 668, 815
Punsly B., Tingay S. J., 2005, ApJ, 633, L89
Richard J., Kneib J., Limousin M., Edge A., Jullo E., 2010, MNRAS, 402, L44
Santos M. R., Ellis R. S., Kneib J., Richard J., Kuijken K., 2004, ApJ, 606, 683
Scarlata C. et al., 2009, ApJ, 706, 1241
Smail I., Ivison R. J., Blain A. W., 1997, ApJ, 490, L5
Smail I., Ivison R. J., Owen F. N., Blain A. W., Kneib J.-P., 2000, ApJ, 528, 612
Smail I., Ivison R. J., Blain A. W., Kneib J., 2002, MNRAS, 331, 495
Solomon P. M., Barrett J. W., 1991, in Combes F., Casoli F., eds, Proc. IAU Symp. 146, Dynamics of Galaxies and Their Molecular Cloud Distributions. Kluwer, Dordrecht, p. 235
Solomon P. M., Vanden Bout P. A., 2005, ARA&A, 43, 677
Solomon P. M., Rivolo A. R., Barrett J., Yahil A., 1987, ApJ, 319, 730
Solomon P. M., Radford S. J. E., Downes D., 1992, Nat, 356, 318
Solomon P. M., Downes D., Radford S. J. E., Barrett J. W., 1997, ApJ, 478, 144
Swinbank A. M. et al., 2008, MNRAS, 391, 420
Tacconi L. J. et al., 2006, ApJ, 640, 228
Tacconi L. J. et al., 2008, ApJ, 680, 246
Valiante E., Lutz D., Sturm E., Genzel R., Tacconi L. J., Lehnert M. D., Baker A. J., 2007, ApJ, 660, 1060

Vernet J., Cimatti A., 2001, A&A, 380, 409
Villar-Martín M., Binette L., Fosbury R. A. E., 1999, A&A, 346, 7
Weiß A., Walter F., Scoville N. Z., 2005, A&A, 438, 533
Weiß A., Downes D., Neri R., Walter F., Henkel C., Wilner D. J., Wagg J., Wiklind T., 2007, A&A, 467, 955
Werner M. W. et al., 2004, ApJS, 154, 1

Yao L., Seaquist E. R., Kuno N., Dunne L., 2003, ApJ, 588, 771
Zhu M., Seaquist E. R., Kuno N., 2003, ApJ, 588, 243

This paper has been typeset from a TEX/LATEX file prepared by the author.